Title

Backbone assignments and conformational dynamics in the S. typhimurium tryptophan synthase α-subunit from solution-state NMR.

Journal

Journal of biomolecular NMR, 74(6-7)

ISSN

0925-2738

Authors

Sakhrani, Varun V
Hilario, Eduardo
Caulkins, Bethany G
et al.

Publication Date

2020-07-01

DOI

10.1007/s10858-020-00320-2

Peer reviewed

HHS Public Access

Author manuscript

J Biomol NMR. Author manuscript; available in PMC 2021 July 01.

Published in final edited form as:

J Biomol NMR. 2020 July ; 74(6-7): 341–354. doi:10.1007/s10858-020-00320-2.

Backbone Assignments and Conformational Dynamics in the *S. typhimurium* Tryptophan Synthase α-Subunit from Solution-State NMR

Varun V. Sakhrani[a], **Eduardo Hilario**[a], **Bethany G. Caulkins**[c], **Mary E. Hatcher-Skeers**[c], **Li Fan**[b], **Michael F. Dunn**[b], **Leonard J. Mueller**[a,*]

[a]Department of Chemistry, University of California Riverside, Riverside, CA 92521, USA

[b]Department of Biochemistry, University of California Riverside, Riverside, CA 92521, USA

[c]Keck Science Department, Claremont McKenna, Pitzer, and Scripps Colleges, Claremont, CA 91711, USA

Abstract

Backbone assignments for the isolated α-subunit of *Salmonella typhimurium* tryptophan synthase (TS) are reported based on triple resonance solution-state NMR experiments on a uniformly ^{2}H, ^{13}C,^{15}N-labeled sample. From the backbone chemical shifts, secondary structure and random coil index order parameters (RCI-S^2) are predicted. Titration with the 3-indole-D-glycerol 3'-phosphate analog, N-(4'-trifluoromethoxybenzenesulfonyl)-2-aminoethyl phosphate (F9), leads to chemical shift perturbations indicative of conformational changes from which an estimate of the dissociation constant is obtained. Comparisons of the backbone chemical-shifts, RCI-S^2 values, and site-specific relaxation times with and without F9 reveal allosteric changes including modulation in secondary structures and loop rigidity induced upon ligand binding. A comparison is made to the X-ray crystal structure of the α-subunit in the full TS αββα bi-enzyme complex and to two new X-ray crystal structures of the isolated TS α-subunit reported in this work.

Keywords

tryptophan synthase; protein NMR; chemical shift assignments; relaxation; protein dynamics; ligand titration

Introduction

The enzyme tryptophan synthase (TS) catalyzes the final two steps in the formation of L-tryptophan from the substrates 3-indole-D-glycerol-3'-phosphate (IGP) and L-serine. X-ray crystallography reveals a 150 Å long linear αββα heterodimer complex with the active sites of the two subunits 25 Å apart and connected by an internal tunnel (Hyde et al. 1988). The α-subunit cleaves IGP via a retro-aldol cleavage reaction into D-glycerol-3'-phosphate (G3P) and indole. Indole then diffuses through the tunnel to the β-subunit (Dunn et al. 1990;

*Corresponding Author: leonard.mueller@ucr.edu.

Hilario et al. 2016), where the pyridoxal-5'-phosphate (PLP) cofactor catalyzes the β-substitution reaction of the L-serine hydroxyl with indole to form L-tryptophan. The smaller, 29-kDa, 268 residue α-subunit is an 8-fold α/β barrel, while the larger β-subunit consists of a helix/sheet/helix domain of 397 residues (Miles et al. 1987; Hyde et al. 1988). Allosteric regulation of substrate channeling between the subunits keeps the two reactions in phase and ensures catalytic efficiency (Barends et al. 2008b; Dunn 2012).

Multiple X-ray crystal structures of the full *S. typhimurium* TS αββα bi-enzyme complex with various α- and β-site ligands (ASL and BSL, respectively) and monovalent cations are available in the Protein Data Bank (PDB) (Kulik et al. 2005; Ngo et al. 2007b; Ngo et al. 2007a; Barends et al. 2008a; Niks et al. 2013). These structures show that the α-subunit of TS has a triosephosphate isomerase (TIM) barrel scaffold with eight parallel β-strands folded into a closed barrel such that each strand is hydrogen-bonded to two neighboring strands with the amino acid sidechains of the barrel defining the hydrophobic core (Figure 1a). The TIM barrel is functionally versatile and the most commonly occurring structure in the PDB database (Wierenga 2001). Eleven solvent-exposed α-helices are interspersed with the β-strands and one of the helices caps the N-terminus of the β-barrel. Like in all TIM-barrel enzymes, the αTS active site is at the C-terminal end of the β-strands and the flexible loops between the α-helices and β-strands sequester the active site from the bulk solvent and aid in substrate binding (Williams and McDermott 1995; Kempf et al. 2007; Wang et al. 2009). Electrostatic field pattern calculations reveal that the backbone atoms build up a positive charge in the region of the active site, correlating the preference of the α-subunit for ligands with negatively charged phosphate groups (Raychaudhuri et al. 1997). From the crystal structure of the TS bi-enzyme complex bound with the IGP analog F9 (PDB IDs: 2CLL, 4HT3), it is observed that the negatively charged phosphate group of the F9 ligand is anchored in the active site via hydrogen bonds with the backbone amides of residues G213, G184, G234, and S235, while the F9 -SO_2 group interacts with the phenolic group of Y175, and the $-CF_3$ and aromatic ring interact with residues A59, L100, L127, A129, I153, Y175, T183, and F212 (Figure 1b), (Ngo et al. 2007a).

In the bi-enzyme complex, αTS switches from an "open" conformation to the catalytically active "closed" state upon binding of its natural substrate or one of its synthetic analogs. In the open state, loop α6β6 (α-L6), comprising residues S178 - L193, is extensively disordered, but upon formation of the closed state the residues forming the loop become well-ordered, as seen in PDB structures 3CEP, 1TJP and 4HPJ (Brzovic et al. 1993; Kulik et al. 2005; Barends et al. 2008a; Fatmi et al. 2009). Structural changes in loop α2β2 (α-L2), comprising residues V52 - D60, are induced by the repositioning of α-L6. The crystal structures show the hydroxyl group of T183 forms a hydrogen bond with D60 (O-O distance ≤ 3.0 Å) in the presence of an α-site ligand (Kulik et al. 2002). Upon IGP binding, α-L2 moves to a position blocking entry to the intramolecular tunnel connecting the α- and β-subunits' active sites, and only after the cleavage of IGP does the loop open to allow diffusion of indole through the tunnel (Brzovic et al. 1993; Harris and Dunn 2002; Dunn 2012). Two allied catalytic mechanisms have been proposed for the α-site reaction. In both models, E49 acts in a "push-pull" acid-base catalytic role while D60 stabilizes the developing charge on the indole ring nitrogen of IGP (Dunn 2012). Mutagenesis studies have established that residues E49 and D60 are critical and have highly conserved catalytic

roles, while T183 and adjacent flexible residues are necessary for allosteric signaling and modulation of the β-site reaction in the TS bi-enzyme complex (Brzovic et al. 1992; Yang and Miles 1992; Rhee et al. 1998; Kulik et al. 2002; Ngo et al. 2007b; Niks et al. 2013).

Both the open and closed conformations of αTS likely preexist in equilibrium even before substrate binding. Following ligand binding, a redistribution of the conformational states occurs, and the ensemble undergoes a population shift favoring the closed conformational states. Both induced fit and conformational selection (Boehr et al. 2009) appear to play roles in this redistribution. In solution, the conformations are in fast exchange, with the observed chemical shifts interpreted as population-weighted averages over the conformations. The interrogation of the isolated αTS (without any allosteric interaction with the β-subunit) both by solution-state NMR spectroscopy and X-ray crystallography permits investigations of these conformational interconversions, providing insight into the behavior of the αTS alone and within the larger context of the full TS $\alpha_2\beta_2$ heterodimer complex.

No X-ray crystal structure of the isolated *S. typhimurium* αTS has been previously reported, but there are structures for the isolated αTS from *E. coli*. (PDB IDs: 1V7Y, 1WQ5) (Nishio et al. 2005). The αTS of *S. typhimurium* and *E. coli* are sequentially 85% identical and play similar roles in the allosteric regulation of the enzymatic activity of the bound β-subunit (Nichols and Yanofsky 1979; Dunn 2012). Partial NMR assignments and secondary structure mapping are also available for the *E. coli* αTS (Vadrevu 2003), and the conformational energy landscape has been investigated via NMR chemical shift projection analysis for ligand titration experiments for site-directed mutants (Axe and Boehr 2013). Yet similar analysis for the *S. typhimurium* αTS is lacking, which is surprising given that the number of crystal structures deposited in the PDB for *S. typhimurium* TS (64 structures) greatly exceed those for *E. Coli* (6 structures).

Here, backbone chemical shift assignments are reported for the *S. typhimurium* αTS based on triple resonance solution-state NMR experiments on a uniformly $^{2}H,^{13}C,^{15}N$-labeled sample. From these, secondary structure and random coil index order parameters (RCI-S^2) are predicted. In addition, the first X-ray crystal structure is reported for the isolated α-subunit of *S. typhimurium* TS. Titration with the ligand F9 leads to perturbations in backbone chemical shifts, assignment probabilities, RCI-S^2, and site-specific relaxation rates that reveal allosteric changes in secondary structures and loop rigidity induced upon ligand binding. These reflect structural and dynamic changes as the protein transitions from the catalytically-inactive open form to the catalytically-active closed conformation, which allows for substrate trapping and efficient in-phase catalysis when attached to the β-subunit (Ngo et al. 2007b; Dunn et al. 2008; Axe and Boehr 2013; Niks et al. 2013; Axe et al. 2014).

Experimental

Protein Expression and Purification:

Uniformly ^{2}H-^{13}C-^{15}N labeled TS from *S. typhimurium* was overexpressed in ampicillin-resistant *E. coli* CB 149 using a multicopy plasmid pEBA-10 carrying the *S. typhimurium* trpA and trpB genes. Cultures were grown at 37 °C in LB until an OD_{600} of 1.4 to 1.6 at half dilution was reached. Cells were then harvested and transferred to minimal media containing

^{2}H-^{13}C-D-glucose, $^{15}NH_4Cl$, and ^{2}H-^{13}C-^{15}N-BioExpress (Cambridge Isotope Labs) dissolved in $^{2}H_2O$. Cells were induced with 1 mM IPTG and allowed to overexpress protein for approximately 18 h at 25 °C. Cells were then collected by centrifugation at 10,000 x g for 30 min. Pellets were resuspended in approximately 50 mL of 50 mM Tris-HCl, pH 7.5, containing 1 mM dithiothreitol (DTT), 5 mM sodium ethylenediaminetetraacetic acid (Na_2EDTA)], and 1 mM phenylmethylsulfonyl fluoride (PMSF) and lysed using sonication. The lysate was centrifuged at 30,000xg at 4 °C for 30 min, and nucleic acids were removed by precipitation with 5 mM spermine followed by centrifugation. From this crude extract labeled TS was crystallized as previously described (Miles et al. 1989; Yang et al. 1992; Caulkins et al. 2014). The purified enzyme was then treated with 1 M KSCN and 0.01 M NH_2OH for 10 min at 22 °C, and the dissociated subunits were loaded onto to a Hiload 16/600 Superdex 200 prep grade size-exclusion column (GE Healthcare Life Sciences) equilibrated with gel filtration buffer (500 mM Bicine, pH 7.4, 1 mM EDTA, 1 mM DTT, 5% (v/v) glycerol and 100 mM NaCl) (Miles and Moriguchi 1977; Miles et al. 1987). The subunits were then eluted at a flow rate of 1ml/min with the AKTA FPLC system and fractions containing the αTS were pooled and buffer exchanged into 50 mM sodium phosphate buffer, pH 6.5, containing 1 mM DTT and 1 mM Na_2EDTA.

NMR spectroscopy:

Chemical Shift Assignments, Secondary Structure Predictions, and RCI-S^2—

Chemical shift assignments for the αTS were obtained using TROSY-based ^{1}H-^{15}N HSQC and triple resonance HNCACB/HN(CO)CACB and HNCO/HN(CA)CO experiments (Riek et al. 2000; Fernández and Wider 2003; Cavanagh et al. 2007). Data were acquired at 25 °C on a Bruker Avance III spectrometer operating at 16.44 T (700 MHz-^{1}H) with a cryogenically cooled probe including Z-axis pulsed field gradients. The protein concentration of the sample was approximately 700-750 μM in pH 6.5, 50 mM sodium phosphate buffer, containing 1 mM DTT, 1 mM Na_2EDTA, 0.05% NaN_3, and 10% (v/v) $^{2}H_2O$. All experiments were conducted with 8 scans per indirect dimension time point and an interscan delay of 1 s. 2D experiments took about 20 minutes whereas each 3D experiment took 1-2 days. Additional acquisition parameters are summarized in Table S1 (ESM).

Spectra were processed using Bruker TOPSPIN version 3.6. Backbone pre-assignments were carried out using strip comparisons and synchronous inspection of NH planes in NMRFAM-SPARKY (Lee et al. 2015). Automated peak picking and probabilistic assignments were respectively carried out using APES (Shin et al. 2006), implemented in NMRFAM-SPARKY, and the PINE algorithm, implemented on the I-PINE webserver (Bahrami et al. 2009; Lee et al. 2019) and accessed via the PINE-SPARKY.2 plug-in (Lee and Markley 2018). The sidechain resonances of Asn and Gln residues (seen in the upper right-hand side of the HSQC spectrum) and the folded peaks from arginine (seen in the lower half of the spectrum) were not assigned. Backbone torsion angle constraints and secondary structure prediction were derived by TALOS-N (Shen and Bax 2013) and secondary chemical shift dependent random coil index (RCI) values were generated and used to obtain quantitative estimates of site-specific order parameters (RCI-S^2) (Berjanskii and Wishart 2005). Using the linear analysis of chemical shifts (LACS) algorithm (Wang et

al. 2005), referencing errors and chemical shift outliers were detected and then used to recalibrate the ^{1}H and ^{13}C chemical shift scales referenced initially with respect to 4,4-dimethyl-4-silapentane-1-sulfonic acid (DSS), used here as an internal standard (Shimizu et al. 1994).

Relaxation Experiments—^{15}N-backbone amide longitudinal relaxation rates (^{15}N-R_1) and in-phase transverse relaxation rates (^{15}N-R_2) of the isolated αTS were measured in the presence and absence of F9 at 700 MHz (^{1}H) and 25 °C using gradient-enhanced phase-sensitive HSQC pulse sequences containing a water flip-back pulse. Delays of 20, 60, 100, 200, 400, 600, 800, and 1200 ms were used for ^{15}N-R_1 experiments, and Carr-Purcell-Maiboom-Gill (CPMG) loop lengths of 29.56, 59.12, 118.24, 236.48, 295.6, 354.72, 413.84, and 472.96 ms were used for ^{15}N-R_2 measurements. Within the interleaved CPMG loop, the delay between the ^{15}N 180° pulses was 900 μs, the ^{15}N pulse width was 160 μs, while the ^{1}H 180° pulse width was 17 μs. Both ^{15}N-R_1 and ^{15}N-R_2 experiments were conducted with 8 transients per increment and an interscan delay of 1 s. Additional acquisition parameters are provided in Table S1. Best-fit relaxation rates were calculated by least-squares fitting of ^{15}N-^{1}H cross-peak intensities to a single-exponential decay in NMRFAM-SPARKY.

CSP Titrations and Estimation of K_d—Chemical shift perturbations were used to estimate K_d by recording a series of ^{1}H-^{15}N HSQC experiments with varying concentrations of F9 ligand and a total protein concentration of 750 μM. After the initial protein-only experiment, F9 was titrated to a final concentration of 50%, 100%, 150%, 200%, 300% and 550% of the total protein concentration. The sample was equilibrated at 25 °C for 15 minutes after each ligand addition. All data were processed and analyzed using the Mestrelab NMR software package (Mestrelab Research).

Molecular Dynamics Simulations

Construction of the ligand-free open αTS: Since the new X-ray crystal structures of the isolated αTS lacks electron density for the dynamic residues in α-L6, the initial structural coordinates of the α-subunit were taken from the X-ray crystal structure of the full TS αββα bi-enzyme complex 4HT3, which has the αTS in the closed conformation. To obtain open conformational structures, the α-subunit was isolated, the α-site ligand removed, and a minimization, equilibration, and 15 ns long MD simulation performed using the generalized Born implicit solvent model (Onufriev et al. 2002) within NAMD 2.13 (Phillips et al. 2005). Open conformations were judged based on the distance between residues T183 (α-L6) and D60 (α-L2) (Fatmi et al. 2009), and were collected and used as starting conformations for further MD simulations.

All-atom MD simulations were performed on the open conformational structures in explicit water (TIP3P model) using the Charmm 36 force field (Huang and Mackerell 2013) within NAMD 2.13 (Phillips et al. 2005). Counterions were added to neutralize the net charge of the system. A 1000-step energy minimization of just the protein using harmonic restraints with a spring constant of 500 kcal/(mol·Å^2) was first performed, followed by a second 1000-step energy minimization using similar restraints on the water molecules. The system was gradually heated in a 100-ps MD simulation from an initial temperature of 0.5 K to a final

temperature of 298 K. The lengths of bonds involving H atoms were fixed by the SHAKE algorithm (Ryckaert et al. 1977). The NPT ensemble and periodic boundary conditions were applied. A temperature of 298 K was maintained using a Langevin thermostat with a damping constant of 2 ps^{-1}, and the hybrid Nose-Hoover Langevin piston method was used to maintain the pressure at 1 atm. The nonbonded interactions were truncated at 14 Å with a switching beginning at 12 Å. Long-range electrostatic interactions beyond the cutoff limit were treated by the particle mesh Ewald method. VMD (Humphrey et al. 1996) was used for visualization and graphical representation. After the simulation reached equilibrium, a 16 ns trajectory was used to generate the structural ensembles. This window size was chosen based on the approximate rotational correlation time for αTS, estimated to be 16 ns at 25° C based on the ^{15}N-R_1/R_2 ratio below (Gu et al. 2014; Pastor and Amero 2015).

In total, 32,000 structures were collected for each of the starting open conformations and used to determine the backbone amide NH bond vector S^2 value for each of the residues (except proline) (Best et al. 2005). Explicit separation of the internal motions from the overall tumbling of the molecule was first achieved by aligning each MD snapshot relative to a reference structure (the first structure of the trajectory). The normalized backbone amide bond vector of each residue was then expressed in Cartesian coordinates ($\hat{\mu} = [x(t),\ y(t),\ z(t)]$), and the ensemble/time average derived S^2-value was calculated from the MD trajectory as (Best et al. 2005):

$$S^2 = \frac{3}{2} tr\left(\langle\ \Phi\ \rangle^2\right) - \frac{1}{2} = \frac{3}{2}\left(\langle x^2\rangle^2 + \langle y^2\rangle^2 + \langle z^2\rangle^2 + 2\langle xy\rangle^2 + 2\langle xz\rangle^2 + 2\langle yz\rangle^2\right) - \frac{1}{2} \quad (1)$$

where the 3 x 3 tensor $\Phi = \hat{\mu} \otimes \hat{\mu}$.

Structural Alignments

Multiple protein structure alignments and calculation of residue-specific RMSD values were carried out using the Multiple Alignment (Eargle et al. 2006) interface to VMD.

X-ray crystallography:

Protein Crystallization and Crystal Structure Determination—αTS was prepared using a modified protocol described in the ESM. Prior to crystallization trials, the αTS sample was centrifuged at 10,000 x g for 20 min at 25 °C to remove aggregates. The Top96 crystallization screen (Anatrace), Art Robbins Intelli-Plate IL96-3, and the Art Robbins Phoenix dispensing system were used to prepare an initial screening plate. Small protein crystals were observed in condition A2 from the Anatrace Top 96 crystallization kit (2 M $(NH_4)_2SO_4$) after 3 days at 25 °C. Fine screening by varying $(NH_4)_2SO_4$ concentration (1.2-1.8 M) in the reservoir yielded larger single crystals. Equal volumes (4 μL) of protein solution (15 mg mL^{-1}) and reservoir solution were mixed and equilibrated against a 500 μL $(NH_4)_2SO_4$ solution in water. Different concentrations of ASL F9 were used during the protein crystallization steps leading to a final concentration in the drop in the range of 2-25 mM. Crystals were grown using a 24-well sitting-drop vapor-diffusion plate (Cryschem M plate, HR1-002, Hampton Research) at 25 °C. Crystals appeared within 3-5 days and grew

up to 14 days as diamond-like crystals. Single crystals (100-150 μm) were soaked in cryoprotectant consisting of the reservoir solution containing up to 30% DMSO and mounted on a nylon loop (Hampton Research, USA). Diffraction data were collected under a gaseous nitrogen stream at 100 K (Oxford Cobra Cryosystems), using X-rays at a wavelength of 1.5418 Å (Rigaku MicroMax-007HF) with the image plate detector Rigaku R-AXIS IV++. Software CrystalClear 2.0 (Rigaku) was used during data collection and X-ray diffraction intensities were processed using iMOSFLM (Leslie 2006) and then scaled with Scala (Evans 2006). The molecular replacement step was performed in Molrep (Vagin and Teplyakov 2010) using the polypeptide chain A from the coordinate file PDB ID: 4KKX as the search model. Crystal structure refinement was performed by iterative cycles of manual inspection of 2Fo-Fc and Fo-Fc electron density maps with Coot (Emsley et al. 2010) followed by structure refinement using the Phenix package (Adams et al. 2010). Data processing statistics are summarized in Table S2 of the ESM. X-ray crystal structures under conditions of 2 mM and 25 mM of F9 were obtained and deposited with the Protein Data Bank under the accession codes 6OSO and 6OUY respectively but no electron density maps for the F9 ligand were observed for either structure.

Results and Discussions

Backbone Chemical Shift Assignments

TROSY-based, triple resonance solution-state NMR experiments (Riek et al. 2000; Fernández and Wider 2003) were used to assign 238 of the 251 non-proline backbone resonances for a U-^{2}H,^{13}C,^{15}N labeled sample of αTS. Triple resonance TROSY-HNCO and TROSY-HN(CO)CACB experiments were used to provide sequential correlations, while TROSY-HN(CA)CO and TROSY-HNCACB were used to both provide intra-residue correlations and confirm sequential assignments.

There were several challenges to the full assignment of the backbone resonances for αTS. In particular, the protein's significant α-helix content (approximately 50%) resulted in substantial chemical shift degeneracy and consequent lack of dispersion in the HSQC spectrum. This led to the regions between 7.5 and 8.7 ppm in the ^{1}H dimension and 117 and 119 ppm in the ^{15}N dimension being overcrowded. To partially combat this, the nitrogen indirect dimension in the 2D HSQC based experiments were run to 51 ms (digital resolution 19.6 Hz). A second challenge arose from the 17 proline residues, which introduced breaks in the sequential linking of the residues. Still, approximately 100 of the backbone resonances were able to be pre-assigned using strip comparisons and synchronous inspection of ^{15}N-^{1}H planes. These were used in concert with automated peak picking and probabilistic assignment using APES (Shin et al. 2006) and the I-PINE webserver (Bahrami et al. 2009; Lee et al. 2019) to assign 238 of the 251 non-proline backbone resonances − 191 with > 99% confidence − as shown in Figures 2 and 3.

Signal broadening due to either conformational dynamics inherent to the loops of the TIM barrel scaffold or to the dynamics arising from the absence of interactions with the β-subunit could be responsible for the low probability and missing resonance assignments in several of the loop regions. In particular, α-L2 and α-L6, located at the interface between the two subunits in the TS bi-enzyme complex and known to become ordered with ligand binding

(Brzovic et al. 1993; Kulik et al. 2005; Fatmi et al. 2009), seem to display intermediate to slow exchange rates for residues comprising the initial portion of these loops. The resultant line broadening of the peaks led to lower probability or complete absence of assignments for these residues. The residues located in the later portion of these loops are presumably in fast exchange and no ambiguities exist in their resonance assignments as shown in Figure 3 (see also Table S3, ESM).

Low probabilities or the complete absence of assignments are also observed for residues in the sequential neighborhood of residues G213, G234 and S235 that hydrogen bond to the negatively charged phosphate group of the active site ligand IGP. This could again be due to conversions between conformational states occurring in the intermediate to slow exchange regime in the absence of substrate. We also note that the HSQC spectrum shows abnormal downfield backbone amide proton (H^N) chemical shifts (>10 ppm) for residues F19, I97, A103, and E134. These can be understood in light of the new X-ray crystal structures reported below in which it is observed that the amide protons of F19, I97, and A103 hydrogen bond to the sidechain δ-oxygen atoms of D46, D124, and D130, respectively, and H^N of E134 hydrogen bonds to an ε-oxygen atoms of its own side chain.

The backbone chemical shifts of ^1H, ^{15}N, and ^{13}C have been deposited at the Biological Magnetic Resonance Bank (BMRB) database (http://www.bmrb.wisc.edu) under accession number 50139.

Prediction of Secondary Structure and Dynamics

Protein secondary structure was predicted based on the combination of the H^N, Cα, Cβ, CO, and N chemical shifts and the protein residue sequence using TALOS-N (Shen and Bax 2013), an artificial neural network-based hybrid system. These are summarized in Figure 4, along with the difference between the Cα and Cβ secondary chemical shifts (Mielke and Krishnan 2009). Probabilistic secondary structure predictions based on backbone chemical shifts were also obtained using PECAN (Eghbalnia et al. 2005) and are provided in Figure S2 (ESM). These can be compared to the secondary structure obtained from the new X-ray crystal structures (PDB IDs: 6OSO, 6OUY), also indicated in Figure 4 and Table S3. The secondary structure predictions from TALOS-N and PECAN agree well with the secondary structure information obtained from X-ray diffraction. However, from the solution-state NMR shifts and TALOS-N the length of the α8' helix is predicted to be reduced from the N-terminal side, with residues 236 to 240 predicted to form a loop instead of the helix seen in the crystal structure. The locations of the α-helices and β-sheets in αTS from *S. typhimurium* also compare well with their counterparts in the isolated *E. coli* αTS (Vadrevu 2003) with the exception that α-L2 for *E.coli* αTS is extended to encompass residues 52 to 77 and the α2' helix does not form (Nishio et al. 2005). The secondary structure information for the isolated αTS closely matches that obtained for the F9 docked α-subunit of the TS αββα bi-enzyme complex (PDB IDs: 2CLL, 4HT3).

Secondary chemical shift dependent random coil index (RCI) values were also generated and then used to obtain quantitative estimates of site-specific order parameters (S^2), predictors of protein backbone rigidity (Berjanskii and Wishart 2005). Order parameters for the backbone amide internuclear bond vector range from 0 to 1, with 0 corresponding to

isotropic motion and 1 indicating complete rigidity relative to the molecular frame (Lipari and Szabo 1982a; Lipari and Szabo 1982b). The RCI-S^2 values are compared to the residue-specific S^2-values from MD in Figure 5. Although there is qualitative agreement, several significant deviations are observed, particularly for regions near the active site. For example, relatively lower RCI-S^2 values are observed for loops α-L2 (residues 52-60) and α-L6 (residues 178-193) and the regions containing residues G213, G234, and S235 that are capable of hydrogen bonding to the negatively charged phosphate group of ASL's. The presence of low RCI-S^2 values signifies dynamic sampling of comparatively more conformations by these residues than predicted by MD and correlates well with the low probabilities or absence of assignments for these same residues. This suggests that these residues undergo longer time-scale motions that are not properly sampled over the limited 16 ns time scale of the MD trajectories. This motion may involve interaction with the phosphate buffer environment of the sample, which was not replicated in the MD simulation. The negatively charged phosphate ions are capable of binding in the αTS active site (Kirschner et al. 1975), and may cause the dynamics of the active site residues to deviate from that captured in the conventional water box MD simulation.

Ligand Binding

Chemical Shift Perturbations and the Ligand Binding Site—The addition of IGP analog F9 led to chemical shift perturbations (CSP's) (Williamson 2013) in the HSQC spectrum of αTS as shown in Figure S3 (ESM). The CSP's were quantified at a protein concentration of 750μM and a [ligand]/[protein] ratio of 3 as the average chemical shift difference $\Delta\delta_{NH}$ (in ppm) from the proton and nitrogen chemical shift perturbations ($\Delta\delta_H$ and $\Delta\delta_N$, respectively), according to the weighted formula (Schumann et al. 2007):

$$\Delta\delta_{NH} = \sqrt{\Delta\delta_H^2 + (0.14\Delta\delta_N)^2} \quad (2)$$

The factor of 0.14 accounts for differences in sensitivity of the amide proton and nitrogen backbone resonances. These are summarized in Figure 6.

The most significant CSPs are found for residues E49, A59, L100, L127, A129, I153, and Y175 and in the proximity of residues F212, G234 and S235, which are marked with asterisks in Figure 6. The relatively high CSPs observed for these residues and their nearest neighbors allow for mapping of the ligand binding site in the isolated αTS (Figure 6b). These can be rationalized in terms of the X-ray crystal structures of the F9 bound full TS complex (Figure 1b), which show residues L100, L127, Y175, and T183 make hydrophobic contacts to the benzene ring of F9, while residues A59, L127, A129, I153, and F212 display hydrophobic interactions with the -CF_3 group. The benzene ring of residue F212 displays pi-pi-interactions with the benzene ring of F9 and the backbone amides of residues G184, G213, G234 and S235 hydrogen bond to the negatively charged phosphate group. The side chain phenolic group of Y175 also hydrogen bonds with the negatively charged -SO_2 group of F9. CSP values for residues F212, G234 and S235 are unavailable due to the absence or low probability of assignments. Residues R15 and G16, present in the initial portion of strand β1, show large CSPs presumably due to perturbed backbone dynamics and

reorganization of the charged sidechains of these residues. The strand β2 residues 49 to 51, located close to the -SO_2 group of F9, also show appreciable changes in chemical shift because of inductive effects experienced in the vicinity of the negatively charged group and because the carboxylate side chain of E49 moves away from its usual catalytic position suited for IGP cleavage. The range of CSP's is small for F9 and αTS, which is attributed in part to the fact that the -CF_3 and -SO_2 groups of F9 can adopt a range of bound conformations, as observed from aligning PDB structures of the full TS complex with F9 (see Figure S4, ESM), and therefore the perturbations in chemical shifts are averaged. From these experiments, we conclude that the binding site for F9 in αTS is not significantly perturbed from that in the full TS complex.

Changes in Dynamics from RCI-S^2 and Relaxation Times—In addition to chemical shift perturbations, the binding of F9 modulates the protein dynamics, reflected in part by subsequent changes in RCI-S^2 values, chemical shift assignment probabilities, and amide backbone R_1 and R_2 relaxation rates. The RCI-S^2 and chemical shift assignment probabilities are tabulated in Table S4 (ESM) and the change in RCI-S^2 upon ligand binding is summarized in Figure 7a, again at a protein concentration of 750μM and a [ligand]/[protein] ratio of 3. The RCI-S^2 of the perturbed chemical shifts show a distinct set of resonances with increased order parameters upon ligand binding that are strongly correlated with the active site. This is highlighted in Figure 7b, in which the change in order parameters is mapped onto the protein residues. Specific regions of note include loop α-L2, located at the interface of the TS αββα bi-enzyme complex, which becomes slightly more ordered, as does the initial portion of loop α-L6 consisting of residues 178 to 184. As observed in the X-ray crystal structure of the TS αββα bi-enzyme complex in the presence of an α-site ligand, the hydroxyl group of T183 (α-L6) forms a hydrogen-bond with D60 (α-L2), resulting in a partially closed loop conformation for α-L6 (visible up to G184). While the region surrounding the ligand appears more ordered upon ligand binding, the regions farther from the active site show increased dynamics.

^{15}N-backbone amide longitudinal (^{15}N-R_1) and transverse (^{15}N-R_2) relaxation rates were also measured before and after the addition of F9 and give an indication (qualitative, here) of the changes in motion occurring in the protein scaffold upon ligand binding (Kay 1998). The experimental data, summarized in Figure 8, highlight that loops α-L2 and α-L6 are more dynamic on the picosecond-to-nanosecond timescale than the rest of the protein, displaying shorter ^{15}N-T_1 relaxation times. The fast bond vector fluctuations happening on this timescale are found to be independent of F9 binding, even in loops α-L2 and α-L6. These observations are consistent with MD simulations, which show that these two dynamic loops sample distinct multiple conformational states in both the presence and absence of F9 (Fatmi et al. 2009), contributing to the retention of entropy during binding of the ASL (Kay et al. 1998; Sapienza and Lee 2010). At the same time, ^{15}N-T_2 relaxation times for the residues in loops α-L2 and α-L6 are found to decrease upon addition of F9. This increase in transverse relaxation rates is consistent with a shift of the conformational sampling between the open and closed conformations toward a single, closed state in the presence of F9, and the subsequent ordering on timescales longer than picosecond-to-nanosecond (Fatmi et al. 2009; O'Rourke et al. 2018).

The ^{15}N-T_1/T_2 ratio also permits an estimation of the overall protein rotational correlation (τ_c) time using the approximation of isotropic rotational diffusion (Kay et al. 1989). Based on the average ^{15}N-T_1/T_2 ratio for select residues in well-defined helices and sheets, the overall rotational correlation time for αTS is estimated to be ~ 16 ns.

Relaxation and exchange experiments probing modulations in the internal motions of αTS mutants from *E. coli* with natural substrates G3P and indole yield similar observations, an expected result as the protein sequences of the αTS for these two species are 85% identical (Axe and Boehr 2013; O'Rourke et al. 2018).

Ligand Titration, Dissociation Constant, and Allosteric Regulation—Ligand titration experiments (Fielding 2007; Williamson 2013) were performed in which the HSQC chemical shifts were followed as a function of the total added ligand, $[F9]_t$. Several representative titration curves are shown in Figure 9 with corresponding spectra in Figure S5 (ESM). The majority of the CSP's shows a characteristic fast exchange, 1:1 binding response (Figure 9a–f) that allows K_d to be obtained by fitting to Equation 3 (Fielding 2007; Williamson 2013):

$$\Delta\delta_{NH} = \Delta\delta_{\max}\frac{([\alpha TS]_t + [F9]_t + K_d) - \sqrt{([\alpha TS]_t + [F9]_t + K_d)^2 - 4[\alpha TS]_t[F9]_t}}{2[\alpha TS]_t} \quad (3)$$

Here $[\alpha TS]_t$ is the total protein concentration, $\Delta\delta_{NH}$ (ppm) is the average chemical shift difference (Equation 2), and $\Delta\delta_{max}$ is the fitted maximum change upon saturation with the ligand. This expression assumes that the exchange between the bound and unbound conformational states is fast. For residues that deviate from fast exchange, the observed shifts are no longer simply the weighted average of free and bound shifts – examples of this are shown in Figures 9g and 9h. The titration curves obtained for these residues have a sigmoidal appearance characteristic of intermediate regime or multi-site binding (Kovrigin 2012). There turns out to be a number of residues in αTS (roughly 1/3 of those that display CSP) that show this behavior

From fitting Equation 3 across the data sets that display fast-exchange binding, an average K_d of 1070±120 μM was obtained. This binding is more than 20 times weaker than that observed for F9 and the full TS heterodimer complex, in which the ligand dissociation constant is 1.84±0.2 μM and 50±5 μM in the presence and absence of L-seine at the β-subunit respectively (Ngo et al. 2007a). This change in binding affinity for the ASL in the presence of a β-site ligand is indicative of allosteric interactions between the two subunits which aid in substrate trapping and effective in-phase catalysis (Ngo et al. 2007b; Dunn 2012; Niks et al. 2013). This is supported by the findings that isolated αTS has an activity that is approximately 30 to 100-fold lower than when bound in the internal aldimine αββα complex and at least 1000 to 3000-fold lower compared to the αββα aminoacrylate form (Kulik et al. 2005). We conclude that the interaction with the β-subunit enables the active site of the αTS to more tightly retain the ligand, although we note that the choice of

phosphate buffer here may complicate the analysis as it may compete for binding with the ASL (Kirschner et al. 1975).

While most peaks showing CSP's are in the 1:1, fast exchange limit, a surprising number of peaks show deviations from fast exchange. Like H92 and A149, these residues tend to be situated at the edges of loops and helices or adjacent to these regions in the tertiary structure (Figure 9i). The locations suggest that these deviations are not the product of a second weak binding event, but rather a manifestation of a longer (millisecond) timescale structural reorganization in response to substrate binding. A number of these residues are located at (what would be) the interface with the β subunit, and we hypothesize that their response is relevant to the allosteric signaling between the α- and β-active sites. Ligand binding at the α-subunit has been shown to activate the rate-determining step in Stage I of the β-site reaction by a factor of 10 (Ngo et al. 2007b; Niks et al. 2013). The millisecond timescale typical for allosteric response is consistent with these residues showing intermediate exchange.

X-Ray Crystal Structures

To place the NMR analysis in context, structural studies of the isolated *S. typhimurium* αTS were also undertaken via X-ray crystallography. Both isolated αTS X-ray crystal structures (PDB IDs: 6OSO and 6OUY) diffracted X-rays to a resolution limit ranging from 1.75 to 1.60 Å. The resolution of the data for refinement purposes was estimated by taking into consideration the completeness of the last resolution shell, $I/\sigma(I)$ ratio, and R_{merge} values. Symmetry analysis indicates that both αTS crystals belonged to the hexagonal space group P 65 2 2 and have near-identical unit-cell parameters and show slight differences in resolution limits (See Table S2, ESM). The calculated value of the Matthews coefficient for both models is identical (Vm = 2.66 $Å^3$ Da^{-1}) and strongly suggests the presence of a single αTS molecule in the asymmetric unit of the crystal with a solvent content of 53.85% and 53.86%, respectively.

Unlike the isolated αTS of *E. coli*, the isolated *S. typhimurium* αTS is observed to preserve its entire secondary structure found when present in the TS bi-enzyme complex. The tertiary structures of αTS show the intact TIM barrel scaffold with an obvious substrate-binding cavity analogous to that observed for the αββα heterodimer complex. However, even in the presence of 25 mM F9 during crystallization, crystals of the isolated αTS did not show the presence of F9 in the active site, confirming that the α-subunit by itself is a much weaker binder compared to the bi-enzyme complex. In addition, some residues (R179 to R188) in loop α-L6 are completely absent in the structure. Without F9 in the active site, we assume that our structure is in the catalytically inactive, open conformation even though we cannot completely see the dynamic segment of loop α-L6. Figure S6 (ESM) shows plots of residue-specific RMSD values for the new X-ray structures of the isolated αTS when aligned structurally to the αTS of the bi-enzyme complex (PDB ID: 4HT3). Very high RMSD values (> 3.5) are observed for residues present in the loops α-L2 and α-L6 and in the immediate neighborhood of residue F107 in helix α−3. As expected, these residues are present at the interface of the TS bi-enzyme complex and in the absence of the β-subunit, these fragments become extremely dynamic and sample many more conformations leading to locally poor-

quality electron density maps or high B values. Low chemical shift assignment probabilities and high predicted RCI-S^2 values and S^2 values from MD trajectories are consistent with the crystallographic studies.

Implications for In-phase, Coupled Catalysis

αTS has evolved in bacteria to cooperate with the beta dimer of TS through formation of the αββα heterodimer for the synthesis of L-tryptophan. In maize, a homolog of αTS, benzoxazineless 1 (BX1) has evolved to synthesize indole via cleavage of IGP for use in an unrelated pathway (Kulik et al. 2005). Free BX1 acts alone, it is not part of a multi-enzyme complex, and it exhibits a turnover rate that is 1400-fold greater than free αTS. The differences in catalytic behavior between αTS and BX1 reflect their differences in biological function. Comparisons of the X-ray crystal structures of BX1 and αTS (Kulik et al. 2005) has led us to hypothesize that the fully realized catalytic activity of BX1 is due to the presence of stabilized α-L2 and α-L6 loops along with the pre-positioning of the active site catalytic residues E49 and D60 in the high activity conformation. Our NMR studies confirm this rigidity is absent in the free αTS. Indeed, for efficient synthesis of L-tryptophan, the activity of αTS is tightly regulated both through assembly of αTS into the αββα heterodimer and via heterotrophic allosteric interactions between the α- and β-sites (Kulik et al. 2005; Dunn 2012).

Conclusion

The residue-wise assignments of backbone C, N and H^N chemical shifts for the isolated αTS of *S. typhimurium* was accomplished using 2D and 3D TROSY-based NMR experiments. These assignments together with relaxation and ligand titration experiments offer insights into the conformational changes of the isolated αTS in solution that are particularly relevant to allosteric regulation involving loops α-L2 and α-L6, proximal to the ASL binding site. The low probability or complete lack of assignments for residues comprising the initial sections of α-L2 and α-L6 correlates with the low order parameters predicted for these same regions. Low probability assignments were also observed for residues that bind to the phosphate group anchor of IGP and other ASL's. The secondary structure observed in our new αTS crystal structures matches that of the full TS bi-enzyme complex and that predicted from TALOS-N and PECAN. RCI predicted and MD derived S^2 values were also low for loops α-L2 and α-L6, which correlate with the absence of α-L6 in the isolated αTS crystal structures.

Titration with the ASL F9 resulted in a reduction in T_2 relaxation times for residues comprising α-L2 and α-L6 while the T_1 relaxation times remained unchanged. We interpret this to be due to a redistribution of conformations of the isolated αTS with the presumed catalytically-active closed conformation becoming more favorable upon ligand binding. The constant T_1 values are consistent with this shift conserving conformational entropy. As the ligand was absent in the X-ray crystal structures of the isolated αTS, the ligand-binding site was mapped from measured CSPs. From changes in chemical shift values alone, the dissociation constant for the binding of F9 to the αTS was determined, and it was observed that without the β-subunit, the alpha active site binds F9 nearly thee orders of magnitude less

tightly than in the TS bi-enzyme complex. These observations underscore the importance of intra-subunit allosteric interactions for the αββα complex and the coordinated regulation of activity at the two subunits that is required for efficient, in-phase catalysis.

Supplementary Material

Refer to Web version on PubMed Central for supplementary material.

Acknowledgments

Research reported in this publication was supported in part by NSF Grant CHE1710671 to L.F. and NIH Grant GM097569 to L.J.M. and M.F.D..

References

Adams PD, Afonine PV., Bunkóczi G, Chen VB, Davis IW, Echols N, Headd JJ, Hung LW, Kapral GJ, Grosse-Kunstleve RW, McCoy AJ, Moriarty NW, Oeffner R, Read RJ, Richardson DC, Richardson JS, Terwilliger TC, Zwart PH (2010) PHENIX: A comprehensive Python-based system for macromolecular structure solution. Acta Crystallogr Sect D Biol Crystallogr 66:213–221 . 10.1107/S0907444909052925 [PubMed: 20124702]

Axe JM, Boehr DD (2013) Long-range Interactions in the Alpha Subunit of Tryptophan Synthase Help to Coordinate Ligand Binding, Catalysis, and Substrate Channeling. J Mol Biol 425:1527–1545 . 10.1016/j.jmb.2013.01.030 [PubMed: 23376097]

Axe JM, Yezdimer EM, O'Rourke KF, Kerstetter NE, You W, Chang CA, Boehr DD (2014) Amino acid Networks in a (β/α)8 Barrel Enzyme Change during Catalytic Turnover. J Am Chem Soc 136:6818–6821 . 10.1021/ja501602t [PubMed: 24766576]

Bahrami A, Assadi AH, Markley JL, Eghbalnia HR (2009) Probabilistic Interaction Network of E vidence Algorithm and its Application to Complete Labeling of Peak Lists from Protein NMR Spectroscopy. PLoS Comput Biol 5:1–15 . 10.1371/journal.pcbi.1000307

Barends TRM, Domratcheva T, Kulik V, Blumenstein L, Niks D, Dunn MF, Schlichting I (2008a) Structure and Mechanistic Implications of a Tryptophan Synthase Quinonoid Intermediate. ChemBioChem 9:1024–1028 . 10.1002/cbic.200700703 [PubMed: 18351684]

Barends TRM, Dunn MF, Schlichting I (2008b) Tryptophan synthase, an allosteric molecular factory. Curr Opin Chem Biol 12:593–600 . 10.1016/j.cbpa.2008.07.011 [PubMed: 18675375]

Berjanskii MV, Wishart DS (2005) A Simple Method to Predict Protein Flexibility Using Secondary Chemical Shifts. J Am Chem Soc 127:14970–14971 . 10.1021/ja054842f [PubMed: 16248604]

Best RB, Clarke J, Karplus M, Pasteur L (2005) What Contributions to Protein Side-chain Dynamics are Probed by NMR Experiments ? A Molecular Dynamics Simulation Analysis. J Mol Biol 349:185–203 . 10.1016/j.jmb.2005.03.001 [PubMed: 15876377]

Boehr DD, Nussinov R, Wright PE (2009) The role of dynamic conformational ensembles in biomolecular recognition. Nat Chem Biol 5:789–796 . 10.1038/nchembio.232 [PubMed: 19841628]

Brzovic PS, Hyde CC, Miles EW, Dunn MF (1993) Characterization of the Functional Role of a Flexible Loop in the α-Subunit of Tryptophan Synthase from Salmonella typhimurium by Rapid-Scanning, Stopped-Flow Spectroscopy and Site-Directed Mutagenesis. Biochemistry 32:10404–10413 . 10.1021/bi00090a016 [PubMed: 8399184]

Brzovic PS, Sawa Y, Hyde CC, Miles EW, Dunn MF (1992) Evidence That Mutations in a Loop Region of the α-Subunit Inhibit the Transition from an Open to a Closed Conformation in the Tryptophan Synthase Bienzyme Complex. J Biol Chem 267:13028–13038 [PubMed: 1618800]

Caulkins BG, Bastin B, Yang C, Neubauer TJ, Young RP, Hilario E, Huang Y- MM, Chang CA, Fan L, Dunn MF, Marsella MJ, Mueller LJ (2014) Protonation States of the Tryptophan Synthase Internal Aldimine Active Site from Solid-State NMR Spectroscopy: Direct Observation of the Protonated Schiff Base Linkage to Pyridoxal-5′-Phosphate. J Am Chem Soc 136:12824–12827 . 10.1021/ja506267d [PubMed: 25148001]

Cavanagh J, Fairbrother W, Palmer III A, Rance M, Skelton N (2007) Protein NMR Spectroscopy: principles and practice, 2nd edn. Elsevier Inc., San Diego

Dunn MF (2012) Allosteric regulation of substrate channeling and catalysis in the tryptophan synthase bienzyme complex. Arch Biochem Biophys 519:154–166 . 10.1016/j.abb.2012.01.016 [PubMed: 22310642]

Dunn MF, Aguilar V, Brzovic P, Drewe WF, Houben KF, Leja CA, Roy M (1990) The Tryptophan Synthase Bienzyme Complex Transfers Indole between the α- and β-Sites via a 25-30 A Long Tunnel. Biochemistry 29:8598–8607 . 10.1021/bi00489a015 [PubMed: 2271543]

Dunn MF, Niks D, Ngo H, Barends TRM, Schlichting I (2008) Tryptophan synthase: the workings of a channeling nanomachine. Trends Biochem Sci 33:254–264 . 10.1016/j.tibs.2008.04.008 [PubMed: 18486479]

Eargle J, Wright D, Luthey-Schulten Z (2006) Multiple Alignment of protein structures and sequences for VMD. Bioinformatics 22:504–506 . 10.1093/bioinformatics/bti825 [PubMed: 16339280]

Eghbalnia HR, Wang L, Bahrami A, Assadi A, Markley JL (2005) Protein energetic conformational analysis from NMR chemical shifts (PECAN) and its use in determining secondary structural elements. J Biomol NMR 32:71–81 . 10.1007/s10858-005-5705-1 [PubMed: 16041485]

Emsley P, Lohkamp B, Scott WG, Cowtan K (2010) Features and development of Coot. Acta Crystallogr Sect D Biol Crystallogr 66:486–501 . 10.1107/S0907444910007493 [PubMed: 20383002]

Evans P (2006) Scaling and assessment of data quality. Acta Crystallogr Sect D Biol Crystallogr 62:72–82 . 10.1107/S0907444905036693 [PubMed: 16369096]

Fatmi MQ, Ai R, Chang CA (2009) Synergistic regulation and ligand-induced conformational changes of tryptophan synthase. Biochemistry 48:9921–9931 . 10.1021/bi901358j [PubMed: 19764814]

Fernández C, Wider G (2003) TROSY in NMR studies of the structure and function of large biological macromolecules. Curr Opin Struct Biol 13:570–580 . 10.1016/j.sbi.2003.09.009 [PubMed: 14568611]

Fielding L (2007) NMR methods for the determination of protein – ligand dissociation constants. Princ Nucl Magnaetic Reson Spectrosc 51:219–242 . 10.1016/j.pnmrs.2007.04.001

Gu Y, Li D- W, Brüschweiler R (2014) NMR Order Parameter Determination from Long Molecular Dynamics Trajectories for Objective Comparison with Experiment. J Chem Theory Comput 10:2599–2607 . 10.1021/ct500181v [PubMed: 26580780]

Harris RM, Dunn MF (2002) Intermediate Trapping via a Conformational Switch in the Na+-Activated Tryptophan Synthase Bienzyme Complex. Biochemistry 41:9982–9990 . 10.1021/bi0255672 [PubMed: 12146962]

Hilario E, Caulkins BG, Huang Y- MM, You W, Chang CEA, Mueller LJ, Dunn MF, Fan L (2016) Visualizing the tunnel in tryptophan synthase with crystallography: Insights into a selective filter for accommodating indole and rejecting water. Biochim Biophys Acta 1864:268–279 . 10.1016/j.bbapap.2015.12.006 [PubMed: 26708480]

Huang J, Mackerell AD (2013) CHARMM36 All-Atom Additive Protein Force Field: Validation Based on Comparison to NMR Data. J Comput Chem 34:2135–2145 . 10.1002/jcc.23354 [PubMed: 23832629]

Humphrey W, Dalke A, Schulten K (1996) VMD: Visual Molecular Dynamics. J Mol Graph 14:33–38 . 10.1016/0263-7855(96)00018-5 [PubMed: 8744570]

Hyde CC, Ahmed SA, Padlan EA, Milesl EW, Davies DR (1988) Three-dimensional Structure of the Tryptophan Synthase α2β2 Multienzyme Complex from Salmonella typhimurium. J Biol Chem 263:17857–17871 [PubMed: 3053720]

Kay LE (1998) Protein dynamics from NMR. Biochem Cell Biol 76:145–152 . 10.1038/755 [PubMed: 9923683]

Kay LE, Muhandiram DR, Wolf G, Shoelson SE, Forman-Kay JD (1998) Correlation between binding and dynamics at SH2 domain interfaces. Nat Strutural Biol 5:156–163

Kay LE, Torchia DA, Bax A (1989) Backbone Dynamics of Proteins As Studied by 15N Inverse Detected Heteronuclear NMR Spectroscopy: Application to Staphylococcal Nuclease. Biochem Cell Biol 28:8972–8979 . 10.1021/bi00449a003

Kempf JG, Jung J, Ragain C, Sampson NS, Loria JP, Haven N (2007) Dynamic Requirements for a Functional Protein Hinge. J Mol Biol 368:131–149 . 10.1016/j.jmb.2007.01.074 [PubMed: 17336327]

Kirschner K, Wiskocil RL, Foehn M, Rezeau L (1975) The Tryptophan Synthase from Escherichia coli. Eur J Biochem 60:513–523 [PubMed: 1107044]

Kovrigin EL (2012) NMR line shapes and multi-state binding equilibria. J Biomol NMR 53:257–270 . 10.1007/s10858-012-9636-3 [PubMed: 22610542]

Kulik V, Hartmann E, Weyand M, Frey M, Gierl A, Niks D, Dunn MF, Schlichting I (2005) On the Structural Basis of the Catalytic Mechanism and the Regulation of the Alpha Subunit of Tryptophan Synthase from Salmonella typhimurium and BX1 from Maize , Two Evolutionarily Related Enzymes. J Mol Biol 352:608–620 . 10.1016/j.jmb.2005.07.014 [PubMed: 16120446]

Kulik V, Weyand M, Seidel R, Niks D, Arac D, Dunn MF, Schlichting I (2002) On The Role of αThr183 in the Allosteric Regulation and Catalytic Mechanism of Tryptophan Synthase. J Mol Biol 324:677–690 . 10.1016/S0022-2836(02)01109-9 [PubMed: 12460570]

Lee W, Bahrami A, Dashti HT, Eghbalnia HR, Tonelli M, Westler WM, Markley JL (2019) I-PINE web server: an integrative probabilistic NMR assignment system for proteins. J Biomol NMR 73:213–222 . 10.1007/s10858-019-00255-3 [PubMed: 31165321]

Lee W, Markley JL (2018) PINE-SPARKY.2 for automated NMR-based protein structure research. Bioinformatics 34:1586–1588 . 10.1093/bioinformatics/btx785 [PubMed: 29281006]

Lee W, Tonelli M, Markley JL (2015) NMRFAM-SPARKY: enhanced software for biomolecular NMR spectroscopy. Bioinformatics 31:1325–1327 . 10.1093/bioinformatics/btu830 [PubMed: 25505092]

Leslie AGW (2006) The integration of macromolecular diffraction data. Acta Crystallogr Sect D Biol Crystallogr 62:48–57 . 10.1107/S0907444905039107 [PubMed: 16369093]

Lipari G, Szabo A (1982a) Model-Free Approach to the Interpretation of Nuclear Magnetic Resonance Relaxation in Macromolecules. 1. Theory And Range Of Validity. J Am Chem Soc 104:4546–4559 . 10.1002/chin.198247060

Lipari G, Szabo A (1982b) Model-Free Approach to the Interpretation of Nuclear Magnetic Resonance Relaxation in Macromolecules. 2. Analysis of Experimental Results. J Am Chem Soc 104:4559–4570 . 10.1021/ja00381a010

Mielke SP, Krishnan V V (2009) Characterization of protein secondary structure from NMR chemical shifts. Prog Nucl Magn Reson Spectrosc 54:141–165 . 10.1016/b978-1-4832-2943-0.50008-x [PubMed: 20160946]

Miles EW, Bauerle R, Ahmed SA (1987) Tryptophan Synthase from Escherichia coli and Salmonella typhimurium. Methods Enzymol 142:398–414 . 10.1016/S0076-6879(87)42051-X [PubMed: 3298982]

Miles EW, Kawasaki H, Ahmed SA, Morita H, Morita H, Nagata S (1989) The β subunit of tryptophan synthase. Clarification of the Roles of Histidine 86, Lysine 87, Arginine 148, Cysteine 170, and Cysteine 230. J Biol Chem 264:6280–6287 [PubMed: 2495283]

Miles WE, Moriguchi M (1977) Tryptophan synthase of Escherichia col. Removal of pyridoxal 5'-phosphate and separation of the alpha and beta2 subunits. J Biol Chem 252:6594–6599 [PubMed: 330534]

Ngo H, Harris R, Kimmich N, Casino P, Niks D, Blumenstein L, Barends TR, Kulik V, Weyand M, Schlichting I, Dunn MF (2007a) Synthesis and Characterization of Allosteric Probes of Substrate Channeling in the Tryptophan Synthase Bienzyme Complex. Biochemistry 46:7713–7727 . 10.1021/bi700385f [PubMed: 17559195]

Ngo H, Kimmich N, Harris R, Niks D, Blumenstein L, Kulik V, Barends TR, Schlichting I, Dunn MF (2007b) Allosteric regulation of substrate channeling in tryptophan synthase: modulation of the L-serine reaction in stage I of the β-reaction by α-site ligands. Biochemistry 46:7740–7753 . 10.1021/bi7003872 [PubMed: 17559232]

Nichols BP, Yanofsky C (1979) Nucleotide sequences of trpA of Salmonella typhimurium and Escherichia coli: an evolutionary comparison. Proc Natl Acad Sci 76:5244–5248 . 10.1073/pnas.76.10.5244 [PubMed: 388433]

Niks D, Hilario E, Dierkers A, Ngo H, Borchardt D, Neubauer TJ, Fan L, Mueller LJ, Dunn MF (2013) Allostery and Substrate Channeling in the Tryptophan Synthase Bienzyme Complex: Evidence for Two Subunit Conformations and Four Quaternary States. Biochemistry 52:6396–6411 . 10.1021/bi400795e [PubMed: 23952479]

Nishio K, Morimoto Y, Ishizuka M, Ogasahara K, Tsukihara T, Yutani K (2005) Conformational Changes in the α-Subunit Coupled to Binding of the β2-Subunit of Tryptophan Synthase from Escherichia coli: Crystal Structure of the Tryptophan Synthase α-Subunit Alone. Biochemistry 44:1184–1192 . 10.1021/bi047927m [PubMed: 15667212]

O'Rourke KF, Axe JM, D'Amico RN, Sahu D, Boehr DD (2018) Millisecond Timescale Motions Connect Amino Acid Interaction Networks in Alpha Tryptophan Synthase. Front Mol Biosci 5:1–10 . 10.3389/fmolb.2018.00092 [PubMed: 29417049]

Onufriev A, Bashford D, Case DA (2002) Modification of the Generalized Born Model Suitable for Macromolecules. J Phys Chem B 104:3712–3720 . 10.1021/jp994072s

Pastor N, Amero C (2015) Information flow and protein dynamics: the interplay between nuclear magnetic resonance spectroscopy and molecular dynamics simulations. Front Plant Sci 6:1–13 . 10.3389/fpls.2015.00306 [PubMed: 25653664]

Pettersen EF, Goddard TD, Huang CC, Couch GS, Greenblatt DM, Meng EC, Ferrin TE (2004) UCSF Chimera - A Visualization System for Exploratory Research and Analysis. J Comput Chem 25:1605–1612 . 10.1002/jcc.20084 [PubMed: 15264254]

Phillips JC, Braun R, Wang W, Gumbart J, Tajkhorshid E, Villa E, Chipot C, Skeel RD, Kalé L, Schulten K (2005) Scalable Molecular Dynamics with NAMD. J Comput Chem 26:1781–1802 . 10.1002/jcc.20289 [PubMed: 16222654]

Raychaudhuri S, Younas F, Karplus PA, Faerman CH, Ripoll DR (1997) Backbone makes a significant contribution to the electrostatics of α/β-barrel proteins. Protein Sci 6:1849–1857 . 10.1002/pro.5560060905 [PubMed: 9300484]

Rhee S, Miles EW, Mozzarelli A, Davies DR (1998) Cryocrystallography and Microspectrophotometry of a Mutant (αD60N) Tryptophan Synthase α2β2 Complex Reveals Allosteric Roles of αAsp60. Biochemistry 2960:10653–10659 . 10.1021/bi980779d

Riek R, Pervushin K, Wüthrich K (2000) TROSY and CRINEPT: NMR with large molecular and supramolecular structures in solution. Trends Biochem Sci 25:462–468 . 10.1016/S0968-0004(00)01665-0 [PubMed: 11050425]

Ryckaert JP, Ciccotti G, Berendsen HJC (1977) Numerical integration of the Cartesian Equations of Motion of a System with Constraints: Molecular Dynamics of n-Alkanes. J Comput Phys 23:327–341 . 10.1016/0021-9991(77)90098-5

Sapienza PJ, Lee AL (2010) Using NMR to study fast dynamics in proteins: Methods and applications. Curr Opin Pharmacol 10:723–730 . 10.1016/j.coph.2010.09.006 [PubMed: 20933469]

Schumann FH, Riepl H, Maurer T, Gronwald W, Neidig KP, Kalbitzer HR (2007) Combined chemical shift changes and amino acid specific chemical shift mapping of protein-protein interactions. J Biomol NMR 39:275–289 . 10.1007/s10858-007-9197-z [PubMed: 17955183]

Shen Y, Bax A (2013) Protein backbone and sidechain torsion angles predicted from NMR chemical shifts using artificial neural networks. J Biomol NMR 56:227–241 . 10.1007/s10858-013-9741-y [PubMed: 23728592]

Shimizu A, Ikeguchi M, Sugai S (1994) Appropriateness of DSS and TSP as internal references for 1H NMR studies of molten globule proteins in aqueous media. J Biomol NMR 4:859–862 . 10.1007/BF00398414 [PubMed: 22911388]

Shin J, Lee W, Weontae L (2006) Structural proteomics by NMR spectroscopy. Proteomics 5:171–185 . 10.1002/0470007745.ch9

Vadrevu R (2003) Partial NMR assignments and secondary structure mapping of the isolated subunit of Escherichia coli tryptophan synthase, a 29-kD TIM barrel protein. Protein Sci 12:185–191 . 10.1110/ps.0221103 [PubMed: 12493842]

Vagin A, Teplyakov A (2010) Molecular replacement with MOLREP. Acta Crystallogr Sect D Biol Crystallogr 66:22–25 . 10.1107/S0907444909042589 [PubMed: 20057045]

Wang L, Eghbalnia HR, Bahrami A, Markley JL (2005) Linear analysis of carbon-13 chemical shift differences and its application to the detection and correction of errors in referencing and spin

system identifications. J Biomol NMR 32:13–22 . 10.1007/s10858-005-1717-0 [PubMed: 16041479]

Wang Y, Berlow RB, Loria JP (2009) Role of Loop-Loop Interactions in Coordinating Motions and Enzymatic Function in Triosephosphate Isomerase. Biochemistry 48:4548–4556 . 10.1021/bi9002887 [PubMed: 19348462]

Wierenga RK (2001) The TIM-barrel fold: a versatile framework for efficient enzymes. FEBS Lett 492:193–198 [PubMed: 11257493]

Williams JC, McDermott AE (1995) Dynamics of the Flexible Loop of Triosephosphate Isomerase: The Loop Motion Is Not Ligand Gated. Biochemistry 34:8309–8319 . 10.1021/bi00026a012 [PubMed: 7599123]

Williamson MP (2013) Using chemical shift perturbation to characterise ligand binding. Prog Nucl Magn Reson Spectrosc 73:1–16 . 10.1016/j.pnmrs.2013.02.001 [PubMed: 23962882]

Yang X-J, Miles EW (1992) Threonine 183 and Adjacent Flexible Loop Residues in the Tryptophan Synthase α Subunit Have Critical Roles in Modulating the Enzymatic Activities of the β subunit in the α2β2 Complex. J Biol Chem 267:7520–7528 [PubMed: 1559990]

Yang XJ, Ruvinov SB, Miles EW (1992) Overexpression and purification of the Separate Tryptophan Synthase α and β Subunits from Salmonella typhimurium. Protein Expr Purif 3:347–354 . 10.1016/1046-5928(92)90011-K [PubMed: 1422228]

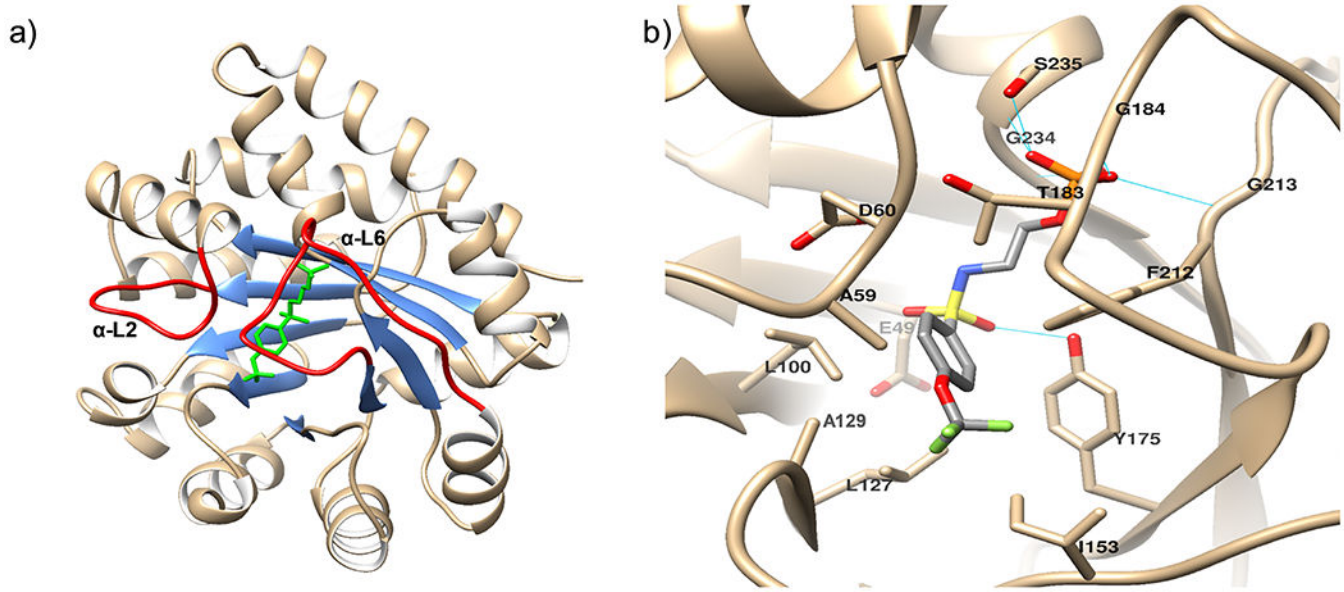

Fig. 1.

(a) Ribbon model of the TS α-subunit from the full $\alpha_2\beta_2$ bi-enzyme complex (PDB ID: 4HT3). The β-strands forming the TIM barrel are shown in blue. Loops α-L6 and α-L2 are shown in red and display the catalytically active "closed" confirmation. The N-(4'-trifluoromethoxybenzenesulfonyl)-2-aminoethyl phosphate (F9) ligand bound in the active site is shown in green. (**b)** Close-up of the active site highlighting sidechains that interact with F9; hydrogen bonds are represented by blue lines. Figure prepared using Chimera (Pettersen et al. 2004)

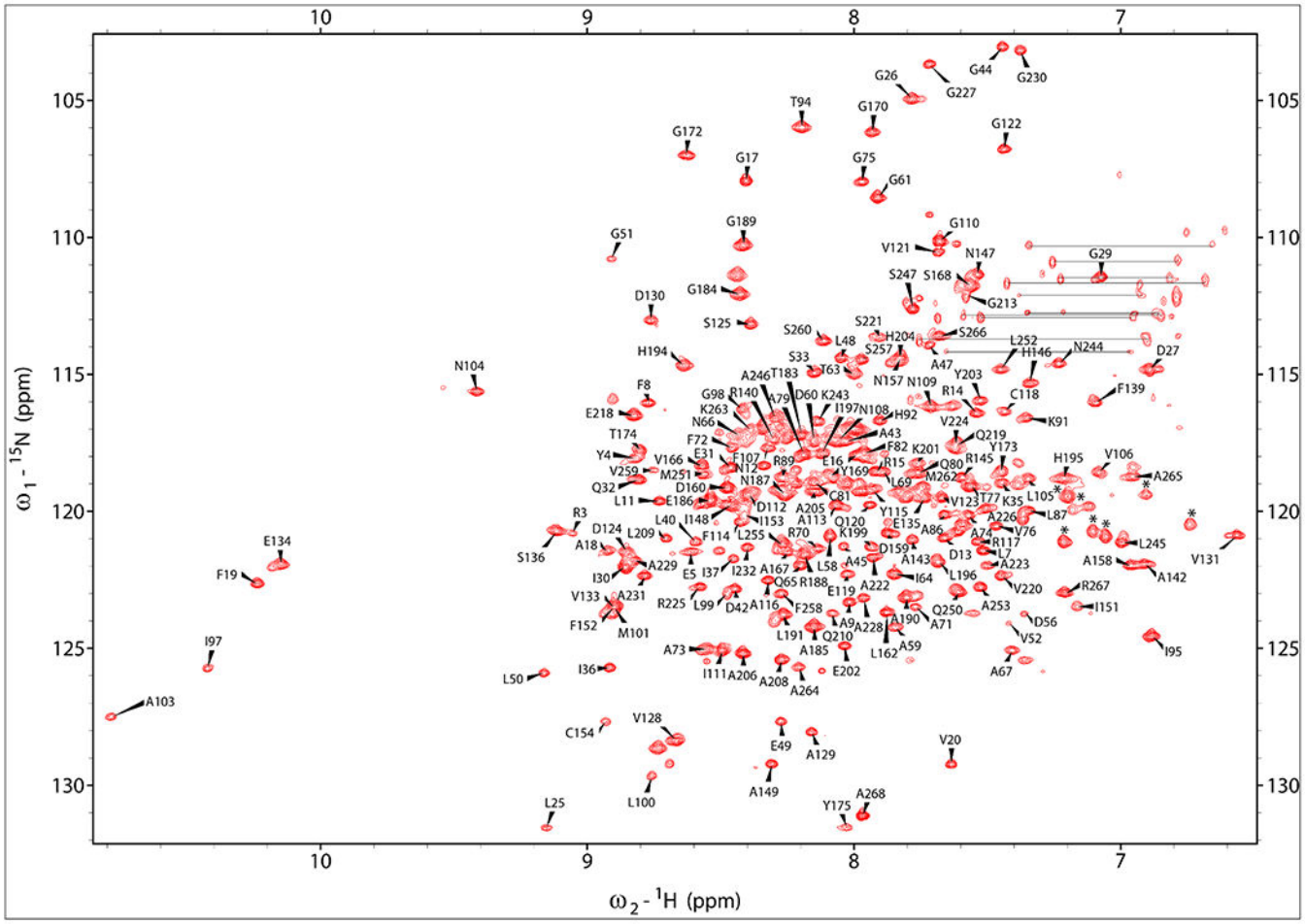

Fig. 2.

Two-dimensional ^{1}H-^{15}N HSQC spectrum of U-^{2}H-^{13}C-^{15}N αTS at 700 MHz, 298K, pH 6.5, and a protein concentration of 750 μM. The 191 labels indicate backbone amide ^{1}H and ^{15}N resonances that could be sequentially assigned with probability > 99%. Peaks connected by thin lines (upper right) correspond to the asparagine and glutamine side chain -NH_2 groups; peaks marked with an asterisk (bottom right) are folded arginine side chain H^{ε}-N^{ε} peaks. The resonance for L127 (δ_{1H} = 8.66 ppm, δ_{15N} = 134.7 ppm) is not shown

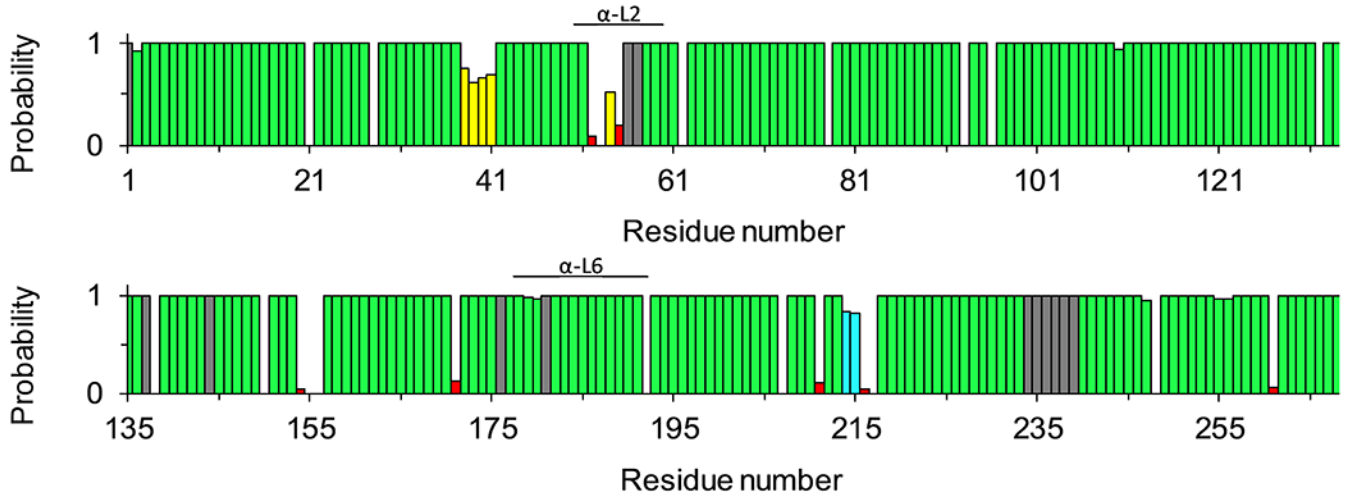

Fig. 3.

Assignment probabilities for each residue of the ligand-free αTS obtained using APES (Shin et al. 2006) and the I-PINE webserver (Bahrami et al. 2009; Lee et al. 2019). Color codes: green bars (> 99%); cyan bars (85% - 99%); yellow bars (50% - 85%); red bars (< 50%); gray bars (no assignment). Loop regions α-L2 and α-L6 are indicated

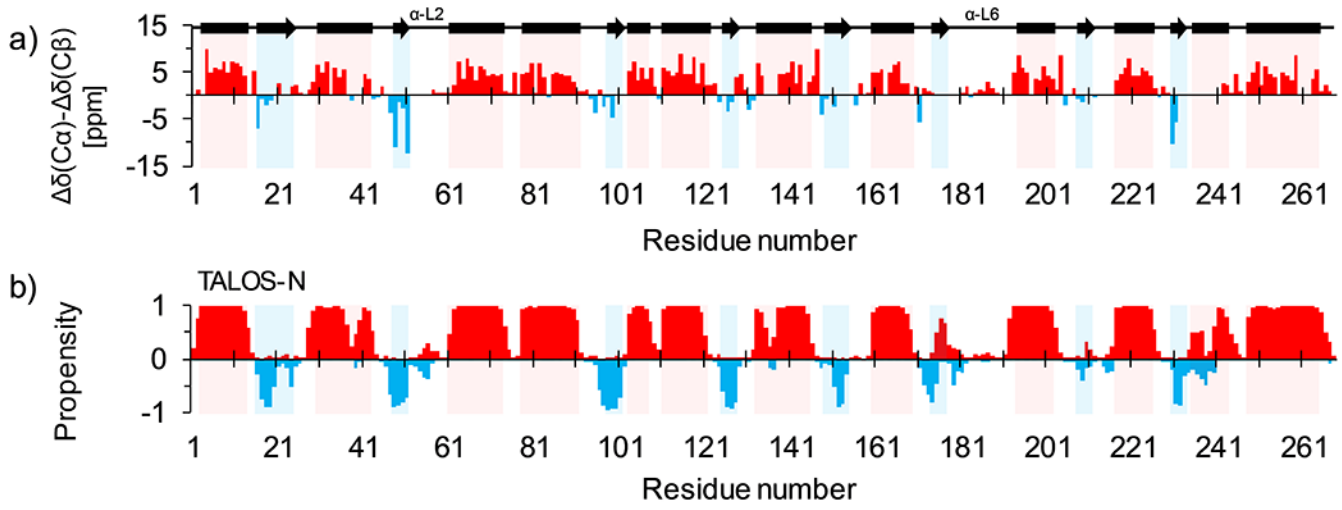

Fig. 4.

(a) Difference between the Cα and Cβ secondary chemical shifts for αTS. **(b)** Secondary structure predictions for αTS from TALOS-N. The propensity of occurrence for α-helix is shown in red and that for β-sheet is shown in blue and inverted. The presence of loops is indicated by the simultaneous presence of helix and strand probabilities. The secondary structure elements from the X-ray crystal structure are indicated across the top (bars α-helices, arrows β-strands) and by the faint red (α-helix) and blue (β-strand) color shades

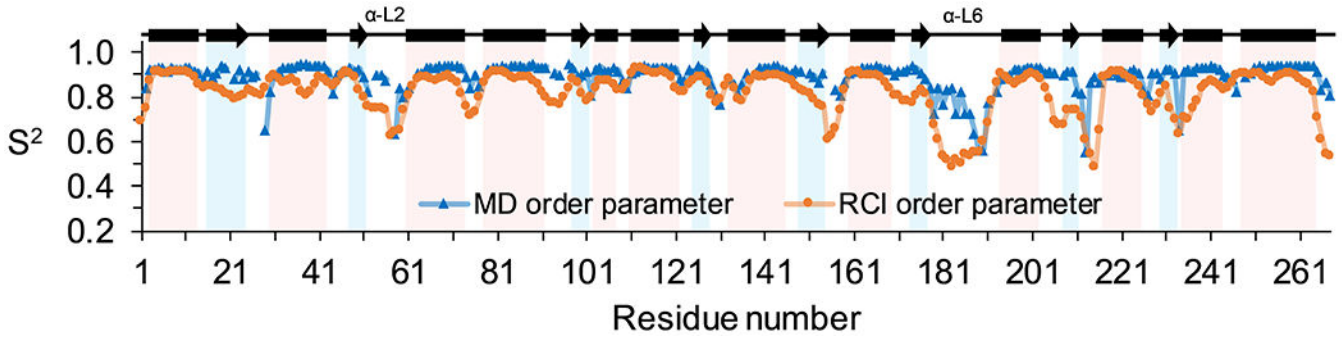

Fig. 5.

RCI-S^2 values of ligand-free αTS (orange circles) compared to the S^2 values calculated from the MD trajectory (blue triangles). The secondary structure elements from the X-ray crystal structure are indicated across the top (bars α-helices, arrows β-strands).

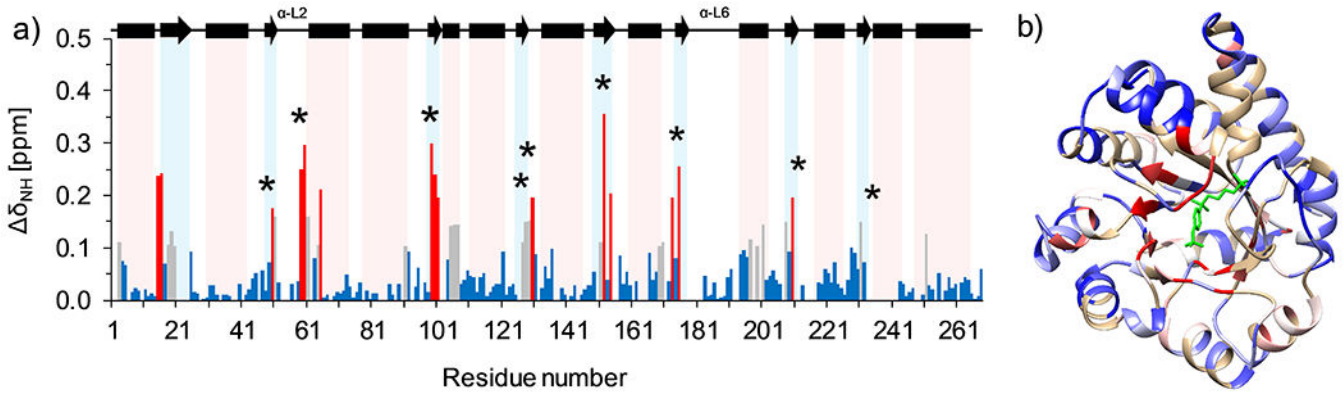

Fig. 6.

(**a)** Average chemical shift changes ($\Delta\delta_{NH}$) calculated for residues of the isolated αTS at a protein concentration of 750 μM and [ligand]/[protein] ratio of 3. Asterisks have been placed over residues E49, A59, L100, L127, A129, I153, and Y175 and also residues F212, G234, and S235 that are seen to interact with F9 in the active site of αTS in the full TS complex and display themselves (or in their sequential neighborhood) relatively large CSPs upon addition of F9. The secondary structure elements from the X-ray crystal structure are indicated across the top (bars α-helices, arrows β-strands). **(b)** Mapping of the αTS ligand binding site onto the isolated αTS structure 6OUY from CSPs. The coordinates for the missing loop α-L6 and the F9 molecule (shown in green) have been extracted from the αTS structure of PDB entry 4HT3 after alignment of both PDB entries. Red indicates residues that show relatively large CSPs, white indicates residues with moderate CSPs, while blue indicates residues with low CSPs

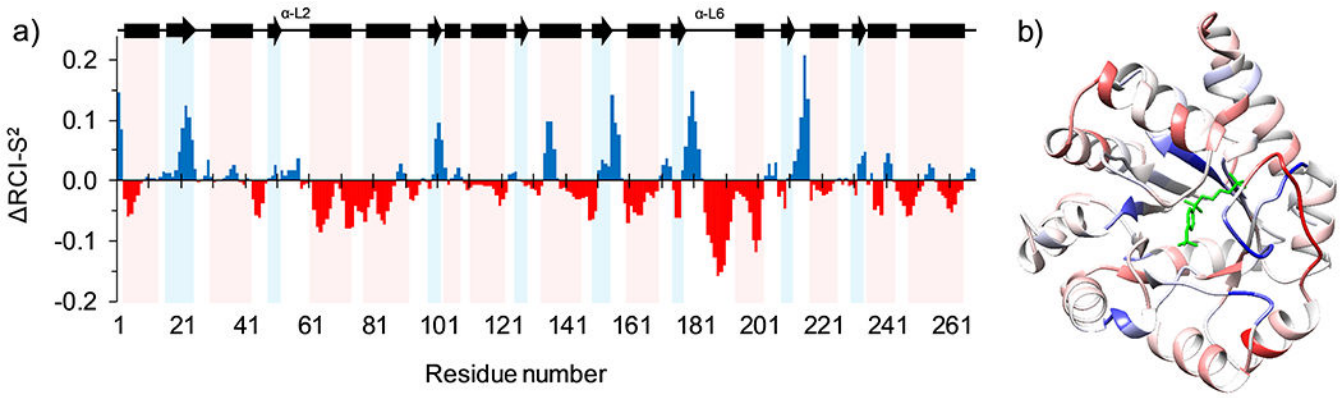

Fig. 7.

(**a)** Difference between RCI-S^2 values for the protein with and without ligand (ΔRCI-S^2) for residues of the isolated αTS at a protein concentration of 750 μM and [ligand]/[protein] ratio of 3. Blue colored upright bars signify increased rigidity and red colored inverted bars decreased rigidity. The secondary structure elements from the X-ray crystal structure are indicated across the top (bars α-helices, arrows β-strands). **(b)** Mapping of the ΔRCI-S^2 values onto the isolated αTS structure 6OUY. The coordinates for the missing loop α-L6 and the F9 molecule (shown in green) have been extracted from the αTS structure of PDB entry 4HT3 after alignment of both PDB entries. Blue indicates increased rigidify while red indicates increased dynamic upon addition of ligand

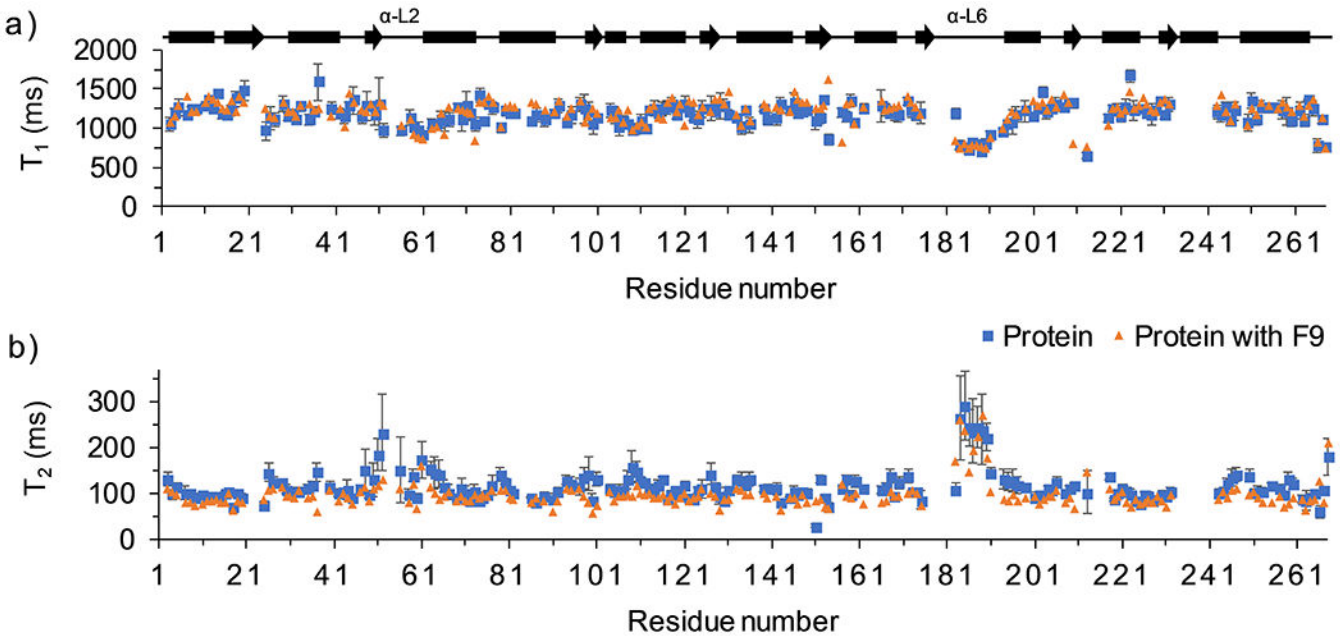

Fig. 8.

Experimental (**a**) ^{15}N-T_1 and (**b**) ^{15}N-T_2 relaxation times for residues of αTS with (orange diamonds) and without (blue squares) F9 at 700 MHz, 298K, a protein concentration of 750 μM, and [ligand]/[protein] ratio of 3. The secondary structure elements from the X-ray crystal structure are indicated across the top (bars α-helices, arrows β-strands)

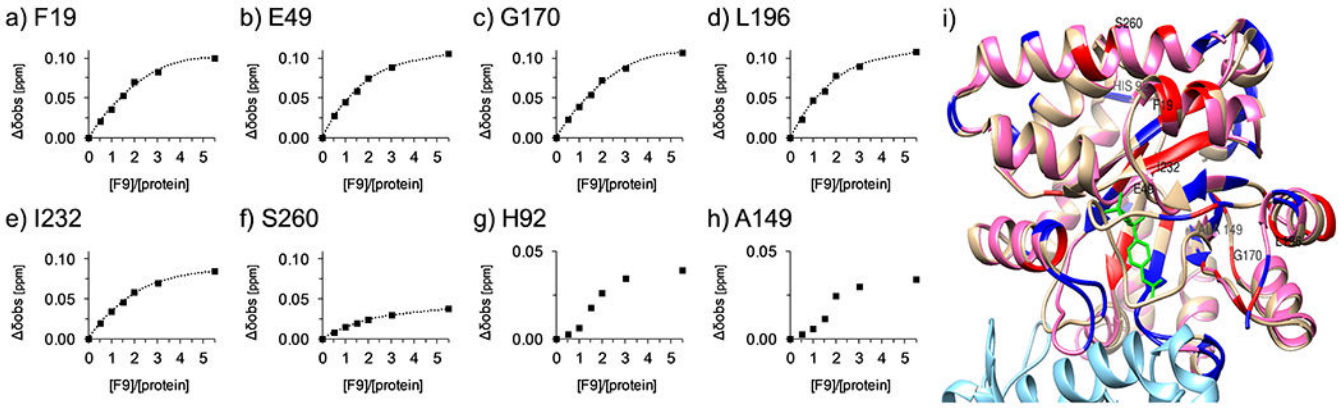

Fig. 9.

Average chemical shift differences (Equation 2) for select residues in αTS displaying fast exchange (**a-f)** and deviations from fast exchange (**g-h)** at a protein concentration of 750μM and [ligand]/[protein] ratios of 0, 0.5, 1, 1.5, 2, 3 and 5.5. (i) Mapping of the residues showing fast (red) and intermediate (blue) exchange onto the isolated αTS (rose; PDBID: 6OSO) aligned with the α-subunit of the αβ dimer (α-subunit, tan; β-subunit, sky blue; PDBID: 4HT3)